Geochemistry, Geophysics, Geosystems

RESEARCH ARTICLE
10.1029/2019GC008448

# Chemical Composition of Carbonate Hardground Cements as Reconstructive Tools for Phanerozoic Pore Fluids

**Andrea M. Erhardt[1], Alexandra V. Turchyn[2], J. A. D. Dickson[2], Aleksey Y. Sadekov[3], Paul D. Taylor[4], Mark A. Wilson[5], Peter Scott[6], and Daniel P. Schrag[7]**

[1]Department of Earth and Environmental Sciences, University of Kentucky, Lexington, KY, USA, [2]Department of Earth Sciences, University of Cambridge, Cambridge, UK, [3]Oceans Institute, University of Western Australia, Crawley, Western Australia, Australia, [4]The Natural History Museum, London, UK, [5]Department of Earth Sciences, The College of Wooster, Wooster, OH, USA, [6]School of Earth Sciences, University of Western Australia, Perth, Australia, [7]Department of Earth and Planetary Sciences, Harvard University, Cambridge, MA, USA

**Key Points:**
- Carbonate hardground cements may capture primary seawater chemistry
- Carbon, oxygen, and strontium isotopes, combined with Mg/Ca and rare earth element abundances, can indicate primary geochemical signals
- Cement chemical evolution can indicate open versus closed system behavior

**Supporting Information:**
- Supporting Information S1
- Table S1

**Correspondence to:**
A. M. Erhardt,
andrea.erhardt@uky.edu

**Citation:**
Erhardt, A. M., Turchyn, A. V., Dickson, J. A. D., Sadekov, A. Y., Taylor, P. D., Wilson, M. A., Scott, P. & Schrag, D. P. (2020). Chemical composition of carbonate hardground cements as reconstructive tools for Phanerozoic pore fluids. *Geochemistry, Geophysics, Geosystems*, *21*, e2019GC008448. https://doi.org/10.1029/2019GC008448

Received 20 MAY 2019
Accepted 7 FEB 2020
Accepted article online 21 FEB 2020
Corrected 26 APR 2020

This article was corrected on 26 APR 2020. See the end of the full text for details.



**Abstract** In this study, we report the chemical composition of early carbonate cement precipitates in carbonate hardgrounds to understand the geochemical signature of near-surface carbonate mineral precipitation. As carbonate hardgrounds lithify at or near the sediment-water interface, they acquire cements that may be minimally evolved from paleoseawater. Using a suite of chemical measurements, we explore the potential of carbonate hardground cements as paleoenvironmental proxies. Trace metal and isotopic ratios, including some rare earth elements, Mg/Ca, manganese, and strontium concentrations, $\delta^{18}O$, $\delta^{13}C$, and $^{87}Sr/^{86}Sr$, were analyzed in the carbonate cements from 17 Phanerozoic carbonate hardgrounds. The sensitivity of the geochemical signal to alteration depends on the geochemical analysis in question and the environmental water-rock ratio. Of these samples, only our modern sample has measurements consistent with primary precipitation from seawater; all other samples precipitated from chemically evolved seawater or were influenced by meteoric water, even if only minimally changed. The more recent samples from the Cenozoic had seawater $^{87}Sr/^{86}Sr$. The Mesozoic samples, in contrast, did not preserve seawater $^{87}Sr/^{86}Sr$, even though the Mg/Ca, $\delta^{18}O$, and $\delta^{13}C$ values were consistent with precipitation from seawater. Finally, the Paleozoic samples preserved expected seawater $^{87}Sr/^{86}Sr$, though rare earth element and $\delta^{18}O$ suggest primary precipitation was from evolved seawater. Additionally, we place our results in the context of open versus closed system precipitation using transects of the Mg/Ca ratios across individual cements. Overall, we stress that one geochemical measurement provides only a partial record of fluid composition, but multiple measurements allow a potential understanding of the seawater geochemical signal.

**Plain Language Summary** All potential archives for reconstructing ancient seawater chemistry have complicating factors, be it biological modification or secondary alteration. This study investigates a promising alternative, carbonate hardground cements. As carbonate hardgrounds form relatively quickly and in equilibrium with seawater, if a sample has remained unaltered, it should retain the primary seawater chemistry. We evaluate 17 samples from across the Phanerozoic, compiling trace element concentrations and isotopic ratios to determine if a sample has undergone significant diagenesis. Overall, no ancient sample satisfies all criteria, but the suite of measurements allows for an evaluation framework for future samples.

## 1. Introduction

Carbonate hardgrounds are rocks that have rapidly lithified at or near the sediment/water interface, resulting from a combination of high carbonate saturation state (Christ et al., 2012; Rameil et al., 2012), low sediment accumulation rate (Kennedy & Garrison, 1975; Shinn, 1969), or elevated fluid flow promoting rapid carbonate mineral precipitation (Dravis, 1979; Lighty, 1985). The rate of lithification of carbonate hardgrounds is variable though short on a geologic timescale (tens to 1,000 years, Christ et al., 2015). Forming at shallow water depths, carbonate hardgrounds are found in warm environments in the modern ocean, such as Pacific atolls (Carpenter et al., 1991), the Arabian Gulf (Khalaf et al., 1987), and the Caribbean (Malone et al., 2001). When sea level falls, carbonate hardgrounds may be subject to meteoric water influence. Carbonate hardgrounds are often identified in the geological record from the subsequent boring and

encrustation by marine organisms of the lithified rock, at least since the beginning of the Phanerozoic (Taylor & Wilson, 2003; Wilson & Palmer, 1992). Most carbonate hardgrounds are clustered in the Mesozoic and Ordovician, with limited occurrences between the Silurian and the Triassic (Christ et al., 2015).

Due to their unique formational environment, the cements that precipitate in carbonate hardgrounds can potentially be restricted in both time and depositional setting. Carbonate hardground cements precipitate within sedimentary pore fluid that is modified from seawater through chemical and biological reactions, typically mediated by subsurface sediment microbial communities (Dupraz et al., 2009; Morse et al., 2007). These cements result in the rapid cementation of carbonate hardgrounds. Because carbonate cements can be chemically evolved from seawater, the geochemical analysis of bulk carbonate rock can contain components that reflect changes in primary seawater chemistry as well as components that reflect changes in pore fluid chemistry; it has been increasingly recognized that bulk geochemical analysis of carbonate rocks may skew a result due to the mixing of multiple geochemically distinct phases (Fike et al., 2015; Friedman & O'Neil, 1977; Givan & Lohmann, 1985; Lohmann & Walker, 1989; Swart, 2015;Tostevin et al., 2016 ; Wallace et al., 2017). Recent advances in laser ablation techniques have allowed microscale geochemical structure to be resolved and individual cement phases to be geochemically interrogated (Tostevin et al., 2016; Wallace et al., 2017). Well-preserved, early marine carbonate cements can be hard to identify in the geological record as their identification requires significant petrographic and geochemical analysis. Additionally, cements can form over a range of depths from the sediment-water interface to deep below the sediment-water interface. Petrographic techniques, including cathodoluminescence, can be used to identify the cement component of a carbonate rock. Within the broader category of carbonate cements, those associated with carbonate hardgrounds may offer the best opportunity of a sedimentary carbonate precipitate that is minimally evolved from seawater given how rapidly many hardgrounds are cemented (Bromley, 1978; Christ et al., 2015; Fursich et al., 1992).

In theory, when the sedimentary precipitation of carbonate minerals begins, the carbonate minerals that precipitate should carry chemical signatures of the formational fluid from which they are derived, namely, pore fluids or porewater, which may be minimally evolved from seawater. The chemical evolution of this pore fluid may leave a distinctive geochemical signature revealing the primary paleo-oceanographic signal. It has been suggested, for example, that uranium concentrations coupled with carbon isotopes and phosphate concentrations in carbonate cements allow both for their identification as cement as well as for reconstruction of pore fluid conditions (Zhao et al., 2016). Carpenter et al. (1991) compared Holocene biogenic carbonate minerals, meaning an allochem that formed from a living organism in the water column, versus abiotic carbonate cement and found they had similar magnesium concentrations, which they interpreted as the carbonate cement reflecting the same chemistry as that of the overlying seawater. This premise was extended to look at the geochemistry of Phanerozoic marine carbonate cements compiled in Dickson (2004), with these results being used to reconstruct changes in major-ion chemistry of the oceans over the Phanerozoic.

Even if the carbonate cement is readily identifiable, many environmental parameters will influence the measured concentration of trace elements or isotope ratios in any carbonate mineral. Factors such as temperature, rate of mineral precipitation, degree of chemical equilibrium between the mineral and fluid, chemistry of the fluid from which the mineral is precipitating, and primary carbonate polymorph control trace element and isotope ratios during mineral formation (Ahm et al., 2018; Brand & Veizer, 1980; Emrich et al., 1970; Friedman & O'Neil, 1977; Swart, 2015; Tostevin et al., 2016; Turner, 1982; Veizer, 1983 and references therein). Of these, the primary carbonate polymorph exerts particular control, as the isotopic fractionation factors and rate of precipitation, as well as the partition coefficients, are drastically different if the initial calcium carbonate polymorph is calcite versus aragonite, versus other structurally different calcium carbonate minerals. Recrystallization of initially precipitated carbonate minerals, which at times are less stable, may then result in secondary changes to the mineral geochemistry. Nearly all carbonate minerals preserved in the geological record are calcite or dolomite; however, it is believed that these minerals precipitated initially as high-Mg calcite or aragonite and, at certain points in Earth history, as calcite directly. Laboratory-defined distribution coefficients of trace elements into carbonate minerals allow us to relate the composition of the carbonate cement with the composition of the fluid from which it precipitates, presuming the carbonate minerals are in equilibrium with the fluid precipitated (Burton & Walter, 1991; Mucci & Morse, 1983; Rimstidt et al., 1998). However, there is a

growing recognition that carbonate minerals are rarely in chemical equilibrium with the fluid from which they precipitated (Nielsen et al., 2013; Watkins et al., 2013). This is in part why the rate of mineral precipitation and the temperature greatly influence the distribution coefficient of trace elements into carbonate minerals during mineral precipitation (Lorens, 1981). Complicating this is the fact that carbonate minerals, cements, and otherwise continue to undergo chemical change as they are buried in a process broadly termed carbonate mineral recrystallization. Different element and isotope ratios have different susceptibilities to diagenetic and epigenetic alteration; therefore, using a suite of geochemical analyses greatly helps with teasing out when and where samples have seen various changes to their geochemical composition (e.g., Cummins et al., 2014).

Here we combine rare earth element (REE) and trace element concentrations, Mg/Ca ratios, $\delta^{18}O$, $\delta^{13}C$, and $^{87}Sr/^{86}Sr$ ratios to explore the geochemistry of carbonate hardground cements over the Phanerozoic. We chose this suite of measurements because they each can be a sensitive recorder of the geochemical changes that occur as you move from seawater to pore water or if the sample was influenced post deposition by meteoric water or broad mineral recrystallization. For example, the incorporation of various REEs into carbonate minerals can indicate precipitation in oxic versus suboxic conditions, where suboxic conditions are typical within sediments and in fluid that is evolved from the bottom water (German & Elderfield, 1990; Li et al., 2019; Wallace et al., 2017). In another example, oxygen isotope ratios and $^{87}Sr/^{86}Sr$ in carbonate minerals are sensitive to the influence of meteoric water, although oxygen isotope ratios in carbonate minerals also vary with temperature (Swart, 2015). The added advantage of measuring $^{87}Sr/^{86}Sr$ is that the $^{87}Sr/^{86}Sr$ of seawater over geological time has varied and is well known (Veizer et al., 1999); therefore, $^{87}Sr/^{86}Sr$ can also be used to help constrain the time of cement precipitation within a temporal geologic context. As a further example, concentrations of strontium and manganese may help to identify carbonate hardground cements that subsequently have undergone recrystallization. Ratios of Mn/Sr ratios, particularly in bulk carbonate samples, have long been used to screen for possible carbonate mineral recrystallization due to the loss of primary strontium and uptake of pore fluid manganese during carbonate recrystallization (Brand & Veizer, 1980; Derry et al., 1992; Veizer et al., 1992). Samples with less than 0.03 weight percent (wt%) strontium and samples with manganese/strontium molar ratios (Mn/Sr) greater than 2 are often identified as nonprimary (Brand & Veizer, 1980; Machel & Buschkuehle, 2008).

The use of multiple geochemical proxies allows us to separate the relative influences of these environmental parameters on the geochemical composition measured in carbonate hardground cements and potentially resolve the fluid chemistry end-member. While carbonate hardgrounds are not immune to recrystallization and alteration, they were chosen for this study with the hope that their rapid lithification near the sediment-water interface makes them a strong candidate for the preservation of initial seawater conditions. This study evaluates multiple Phanerozoic samples to evaluate the reliability of hardgrounds as a paleoseawater proxy.

## 2. Materials and Methods

Samples of carbonate hardgrounds were obtained from the collections of Natural History Museum (London), The College of Wooster, the University of Colorado, Eötvös Loránd University, University of Saskatchewan, and the University of Cambridge. Samples are from the modern, Holocene, Oligocene, Cretaceous, Jurassic, Triassic, Permian, Carboniferous, Ordovician, and Cambrian. The samples used in this study, including their ages, locations, reference for their depositional environment, and description of their depositional environment, are given in Table 1. Of the 17 samples in this study, 15 are from classic intertidal and subtidal beach environments, and two likely formed in deeper water environments. Representative thin section images are shown in Figure 1.

Elemental ratios were determined using the Cameca SX100 electron microprobe analyzer at the University of Cambridge, on polished 30 μm thin sections. The detection limits for calcium, aluminum, sulfur, strontium, magnesium, iron, manganese, and silica are determined based on matrix-matched standard calibrations, and the standard deviation of individual measurements are typically less than 100 ppm for magnesium and 250 ppm for calcium (supporting information Table S1). To convert the measured Mg/Ca ratios in the authigenic carbonate to formational fluid composition, the distribution coefficient ($K_D$) was calculated using the formula from Rimstidt et al. (1998):

**Table 1**
*Samples Used in This Study*

| | Age (Ma) | Stage | Period | Location | Reference | Depositional environment |
|---|---|---|---|---|---|---|
| 1 | 0 | Modern | Neogene | Enewetak Atoll, Marshalls Islands | Carpenter et al. (1991) | Shallow water modern Atoll, classic beachrock; carbonate environment |
| 2 | 0.0007 | Late Holocene | Neogene | Intertidal Zone, Persian Gulf, UAE | Paul and Lokier (2017) | Carbonate intertidal zone |
| 3 | 0.006 | Early Holocene | Neogene | Mussafah Channel Hardground, UAE | Paul and Lokier (2017) | Carbonate intertidal zone |
| 4 | 35 | Lower Oligocene | Neogene | Suwannee Limestone, USA | Budd (2002) | Formation has tidal structures and evaporite minerals, dominantly carbonate |
| 5 | 42 | Middle Eocene | Paleogene | Avon Park Formation, USA | Budd (2002) | Shallow water, with tidal structures and evaporites; carbonate system |
| 6 | 66 | Maastrichtian 1 | Cretaceous | Meerssen Member, the Netherlands | Van der Ham et al. (2007) | From the type section for the Mastrictian; seagrass present, predominantly carbonate minerals |
| 7 | 125–129 | Aptian-Barremian | Cretaceous | Qishn Formation, Oman | Immenhauser et al. (2004) | Shallow-water cycle tops, likely intertidal, carbonate-dominated |
| 8 | 100 | Cenomanian | Cretaceous | Upper Greensands, Devon, UK | Gallois (2005) | Subtidal carbonate |
| 9 | 145–161 | Valanginian | Jurassic | Gerecse Mts. of Hungary | Jenkyns and Clayton (1986) | Deepwater sediment, pelagic "red" limestone, clays |
| 10 | 145–161 | Valanginian | Triassic | Gerecse Mts. of Hungary | Jenkyns and Clayton (1986) | Deepwater sediment, pelagic "red" limestone, clays |
| 11 | 242 | Triassic | Triassic | Latimar Formation | Christ et al. (2012) | Classic peritidal cycle top carbonate hardgrounds |
| 12 | 299–305 | Kasimovian | Pennsylvanian/ Carboniferous | Holder formation, New Mexico | Goldstein (1988) and Wasson and Lohman (2015) | Algal Mounds and tidal structures suggest tidal environment; carbonate dominated |
| 13 | 299–305 | Kasimovian | Pennsylvanian/ Carboniferous | Holder formation, New Mexico | Goldstein (1988) and Wasson and Lohman (2015) | Algal Mounds and tidal structures suggest tidal environment; carbonate dominated |
| 14 | 331–347 | Visean | Carboniferous | Eskett Limestones, England | Dean et al. (2011) | From a cycle top—often calcrete (subaerially exposed) |
| 15 | 461–468 | Dariwillian | Ordovician | Kanosh Formation, Utah | McDowell (1995) | Intertidal and subtidal carbonate sedimentation; mixed carbonate-clastic environment |
| 16 | 485–497 | Furongian | Cambrian 1 | Furongian, Banff National Park | Westrop (1989) | Subtidal, storm dominated shelf, dominantly carbonate |
| 17 | 495–505 | Drumian | Cambrian 2 | Marjuman, Banff National Park | Aitken (1978) | Peritidal carbonates |

$$\log K_D\left(\frac{Mg}{Ca}\right) = 4.436 - \left(\frac{1348}{T}\right) - 0.005339T,$$

where T is temperature in Kelvin. This relationship was empirically derived and presumes near-equilibrium conditions, the assumption for most natural systems (Rimstidt et al., 1998). This equation was also used in other studies of trace element partitioning into abiotically precipitated carbonates, namely, the carbonate vein studies of Coggon et al. (2010) and Rausch et al. (2013). Other distribution equations, such as those of Burton and Walter (1991) and Mucci and Morse (1983), show similar relationships for temperature and $K_D$, though absolute values vary slightly. Temperature ranges of 15–35 °C were used to encompass the likely range of shallow marine carbonate formation.

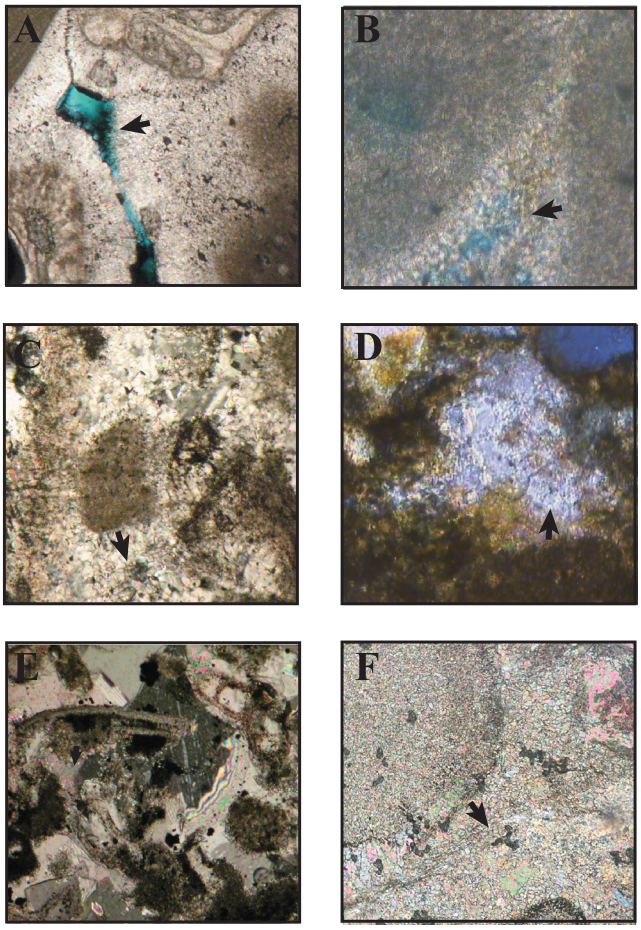


**Figure 1.** Representative thin section images from samples in this study. Arrows show the horizon of sample collection. Sample ages and descriptions: (a) Modern, Enewetak Atoll, fibrous high Mg calcite; (b) Oligocene Suwannee Limestone, radial axial and microcrystalize low Mg calcite; (c) Maastrichtian Meerssen Member, dogtooth low-Mg calcite with blocky pore-filling calcite; (d) Jurassic Gerecse Mountains, microcrystalline early calcite with blocky pore-filling calcite; (e) Pennsylvanian Holder Formation, microcrystalline calcite around grain edges; and (f) Cambrian, Marjumam age, Pika formation, microcrystalline and drusy calcite. Images (a) and (e) were taken at 4X magnification, while Images (b), (c), (d), and (f) were taken at 10X magnification.

Trace element profiles, including selected light REEs plus yttrium (hereafter REY), were measured using an Analyte G2 excimer laser (Teledyne Photon Machines Inc, Omaha, NE, USA) coupled with Thermo i-CapQ ICP-MS at the University of Cambridge, following the methods later outlined in Gabitov et al. (2017) and Skinner et al. (2019). Only selected REYs were measured because of counting statistics at the time of analysis. The internal reproducibility of the primary standard (NIST-SRM614, glass) was on average 0.4% RSD 1$\sigma$, while the reproducibility of the secondary standard (internal eBlue, carbonate) was 1.5% RSD 1$\sigma$. The differences between these are likely due to inhomogeneity of the carbonate material. Further information on long-term internal and external precision are outlined in Skinner et al. (2019). Our results are normalized to post Archean Australian Shale (Pourmand et al., 2012) to allow for comparison with average crustal values. In this study, Ce anomalies were calculated using the formula from Lawrence et al. (2006) to minimize the potential influence of anomalous behavior of La (Bau & Dulski, 1996). The equation used is as follows:

$$Ce_{SN}/Ce^{*}_{SN} = \frac{[Ce]_{SN}}{([Pr]_{SN})^{2}/[Nd]_{SN}}.$$

Thresholds of 1.1 and above were used to denote a positive Ce anomaly (deposition in anoxic conditions) and below 0.9 to indicate a negative Ce anomaly (deposition in oxic conditions) as applied in Tostevin et al. (2016); the use of the Ce anomaly allows us to better compare results from samples with such widely varying absolute REY concentrations. Data acquired using laser ablation transects have a degree of variability between each individual measurement, resulting in calculations of Ce anomalies that vary. Point measurements, in contrast, allow for longer dwell times and higher counts and are therefore theoretically more reliable measurements. As a result, only point measurements are considered for Ce-anomaly analysis.

Samples for bulk strontium isotopes ($^{87}Sr/^{86}Sr$) were collected using a tungsten needle with a 1 μm point through scraping, allowing for the collection of only the authigenic carbonate phase (Dickson et al., 2008). The strontium was separated from the carbonate matrix using Eichron strontium spec resin. The strontium isotope ratios of this separated fraction were analyzed on a Thermo Scientific Triton Plus Multicollector Thermal Ionization Mass Spectrometer (TIMS) using double rhenium filaments. The NIST 987 standard was run, bracketing every four to five samples, and the reproducibility of the standard was 5 ppm. Additional high-resolution measurements of $^{87}Sr/^{86}Sr$ were collected using laser ablation on polished 30 μm thin sections and measured on the Neptune Plus Multicollector Inductively Coupled Plasma Mass Spectrometer (Christensen et al., 1995). In this case, the Analyte G2 excimer laser (Teledyne Photon Machines Inc, Omaha, NE, USA) is connected such that the laser-ablated samples are input directly into the Neptune plasma. Both systems were optimized for signal stability. Spot sizes for laser ablation strontium isotope analysis were either 50 or 100 μm, depending on the width of authigenic carbonate available, and were calibrated with similar spot sizes using four in-house standards (eBlue, NCC, OKA, and Par), which were measured and calibrated separately on the Triton TIMS at the University of Cambridge and match within 50 ppm of the $^{87}Sr/^{86}Sr$ measured on the TIMS. Overall, 62 discrete 100 μm diameter points and 53 discrete 50 μm diameter points were measured for $^{87}Sr/^{86}Sr$ via laser ablation-Neptune.

Oxygen and carbon isotope ratios were measured on the tungsten-needle manually separated samples using a dual-inlet Thermo MAT253 with Finnigan Gas Bench II in the Godwin Laboratory at the University of

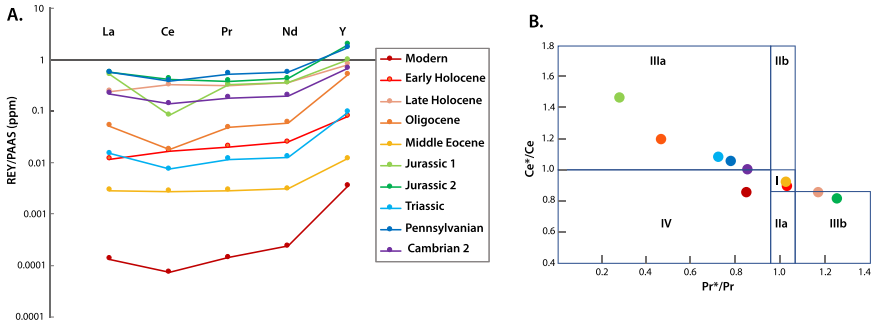


**Figure 2.** Average measurements of REY profiles for 10 carbonate hardground samples. (a) shows the abundances of La, Ce, Pr, Nd, and Y normalized to PAAS. (b) is a Ce anomaly versus Pr anomaly diagram after Hu et al. (2014). The zones are as follows: Field I = no anomaly; Field IIa = positive La anomaly produces an apparent negative Ce anomaly; Field IIb = a negative La anomaly causes an apparent positive Ce anomaly; Field IIIa = real positive Ce anomaly; Field IIIb = real negative Ce anomaly; Field IV = positive La anomaly disguises a positive Ce anomaly.

Cambridge. The results are reported with reference to the international standard VPDB for carbon and oxygen, with precision better than ±0.08‰ for $\delta^{13}C$ and ±0.10‰ for $\delta^{18}O$.

## 3. Results

### 3.1. REY

Two hundred spot points and 24 transects were measured for La, Ce, Pr, Nd, and Y, which are collectively termed the light REY. The samples analyzed for this study exhibit a wide range of concentrations of the REE measured varying over many orders of magnitude (1 to 0.0001; Figure 2a). Samples range in Ce anomalies from positive to negative (Table 2 and Figure 2b). The full data table with all analyses is given in Supporting Information S1.

### 3.2. $\delta^{13}C$ and $\delta^{18}O$

The carbon and oxygen isotopic composition of the carbonate hardground cements is lower for older samples (Table 3 and Figure 3). Paleozoic samples have much more negative $\delta^{18}O$, ranging from −6‰ to −11‰. The $\delta^{13}C$ ranges between approximately −5‰ and +3.5‰. When $\delta^{13}C$ and $\delta^{18}O$ are cross-plot in Figure 3, the general relationship between more positive $\delta^{13}C$ and $\delta^{18}O$ in more recent samples and more negative $\delta^{13}C$ and $\delta^{18}O$ for older samples is observed.

### 3.3. Strontium Isotopes

Average results for $^{87}Sr/^{86}Sr$ are given in Table 3 and detailed results in Table S1. Both samples analyzed by TIMS and by LA-MC-ICPMS were comparable, supporting the ability to measure $^{87}Sr/^{86}Sr$ by LA-MC-ICP-

**Table 2**
*Average PAAS Normalized REY Concentrations in ppm*

| Age (Ma) | Stage | Period | $La_{SN}$ | $Ce_{SN}$ | $Pr_{SN}$ | $Nd_{SN}$ | $Y_{SN}$ | $Ce_{SN}/Ce_{SN}^*$ |
|---|---|---|---|---|---|---|---|---|
| 0 | Modern | Neogene | 0.0001 | 0.0001 | 0.0001 | 0.0002 | 0.0035 | 0.84 |
| 0.0007 | Late Holocene | Neogene | 0.24 | 0.33 | 0.32 | 0.35 | 0.79 | 1.16 |
| 0.006 | Early Holocene | Neogene | 0.01 | 0.02 | 0.02 | 0.03 | 0.08 | 1.02 |
| 35 | Lower Oligocene | Neogene | 0.05 | 0.02 | 0.05 | 0.06 | 0.51 | 0.46 |
| 35 | Lower Oligocene | Neogene | 0.00 | 0.00 | 0.00 | 0.00 | 0.01 | 1.02 |
| 145–161 | Valanginian | Jurassic | 0.51 | 0.08 | 0.33 | 0.36 | 0.99 | 0.28 |
| 145–161 | Valanginian | Jurassic | 0.57 | 0.42 | 0.38 | 0.43 | 1.92 | 1.25 |
| 242 | Triassic | Triassic | 0.01 | 0.01 | 0.01 | 0.01 | 0.09 | 0.72 |
| 299–305 | Kasimovian | Pennsylvanian/Carboniferous | 0.57 | 0.38 | 0.53 | 0.56 | 1.70 | 0.78 |
| 495–505 | Drumian | Cambrian 2 | 0.20 | 0.16 | 0.18 | 0.20 | 0.66 | 1.02 |

*Note*. SN as a subscript refers to "shale normalized."

Geochemistry, Geophysics, Geosystems

10.1029/2019GC008448

**Table 3**
*Isotopic Measurements for $^{87}Sr/^{86}Sr$, $\delta^{18}O$, and $\delta^{13}C$ for Carbonate Cements*

| | Age (Ma) | Stage | Period | Location | $^{87}Sr/^{86}Sr$ (laser, # of measurements) | $^{87}Sr/^{86}Sr$ std dev (laser) | $^{87}Sr/^{86}Sr$ (cements- TIMS) | $^{87}Sr/^{86}Sr$ std dev (TIMS) | $\delta^{18}O_{VPDB}$ | $\delta^{13}C_{VPDB}$ |
|---|---|---|---|---|---|---|---|---|---|---|
| 1 | 0 | Modern | Neogene | Enewetak Atoll, Marshalls Islands | 0.70920 (6) | 4.8E−05 | 0.70924 | 4.8E−05 | −0.97 | 3.42 |
| 2 | 0.0007 | Late Holocene | Neogene | Intertidal Zone, Persian Gulf, UAE | 0.70920 (18) | 4.4E−05 | 0.70920 | 3.4E−05 | −1.46 | 1.74 |
| 3 | 0.006 | Early Holocene | Neogene | Mussafah Channel Hardground, UAE | 0.70916 (8) | 1.4E−05 | 0.70918 | 1.2E−05 | 2.75 | 1.50 |
| 4 | 35 | Lower Oligocene | Neogene | Suwannee Limestone, USA | 0.70801 (11) | 2.8E−04 | | | −2.56 | 0.27 |
| 5 | 42 | Middle Eocene | Paleogene | Avon Park Formation, USA | 0.70785 (17) | 3.7E−04 | | | — | — |
| 6 | 66 | Maastrichtian | Cretaceous | Meerssen Member, the Netherlands | | | 0.70786 | 3.5E−06 | −0.69 | 1.49 |
| 7 | 125–129 | Aptian-Barremian | Cretaceous | Qishn Formation, Oman | | | 0.70782 | 3.5E−06 | −1.37 | −5.15 |
| 8 | 100 | Cenomanian | Cretaceous | Upper Greensands, Devon, UK | | | 0.70769 | 3.5E−06 | −2.02 | 2.69 |
| 9 | 145–161 | Valanginian | Jurassic | Gerecse Mts. of Hungary | 0.70797 (6) | 1.2E−03 | 0.70840 | 9.4E−04 | 0.57 | 2.44 |
| 10 | 145–161 | Valanginian | Jurassic | Gerecse Mts. of Hungary | 0.70764 (11) | 6.0E−04 | 0.70763 | 3.6E−04 | −0.32 | 3.10 |
| 11 | 242 | Triassic | Triassic | Latemar Formation | 0.70781 (12) | 2.6E−04 | | | −5.77 | 1.63 |
| 12 | 299–305 | Kasimovian | Pennsylvanian/ Carboniferous | Holder formation, New Mexico | 0.70893 (10) | 4.4E−04 | 0.70900 | 2.8E−04 | −5.93 | 2.20 |
| 13 | 299–305 | Kasimovian | Pennsylvanian/ Carboniferous | Holder formation, New Mexico | | | | | | |
| 14 | 331–347 | Visean | Carboniferous | Eskett Limestones, England | | | 0.70852 | 3.5E−06 | −7.55 | −1.47 |
| 15 | 461–468 | Dariwillian | Ordovician | Kanosh Formation, Utah | | | 0.70978 | 3.5E−06 | −7.93 | −2.80 |
| 16 | 485–497 | Furongian | Cambrian 1 | Furongian, Banff National Park | | | 0.71074 | | −10.42 | 0.54 |
| 17 | 495–505 | Drumian | Cambrian 2 | Marjuman, Banff National Park | 0.714381 (15) | 2.1E−03 | | | −8.44 | 0.03 |

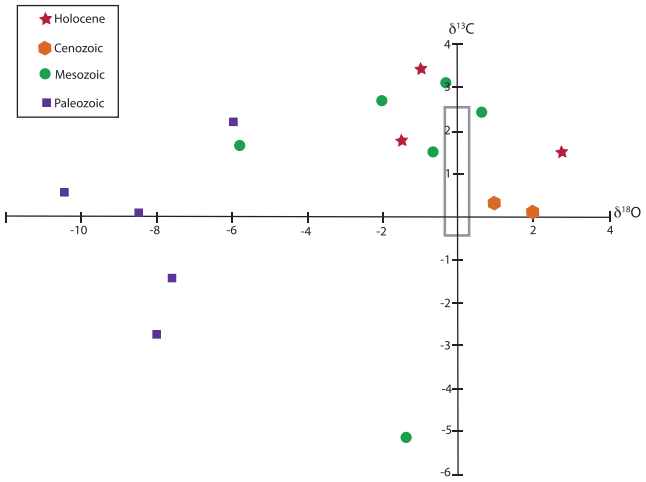


**Figure 3.** Cross-plot of $\delta^{18}O_{VPDB}$ and $\delta^{13}C_{VPDB}$ for carbonate hardground cements from this study. Holocene samples are represented in red, Cenozoic samples in orange, Mesozoic samples in green, and Paleozoic samples in purple. The box denotes where modern carbonate minerals precipitate in carbon-oxygen isotope space.

MS. Results ranged from 0.7076 to 0.7107 for $^{87}Sr/^{86}Sr$. These values are then compared to the established seawater $^{87}Sr/^{86}Sr$ curve and will be discussed later (Figure 4).

### 3.4. Element Concentrations and Ratios

Average manganese concentrations and Mn/Sr are given in Table 4. Concentrations ranged from 1 to 850 ppm, with standard deviations for all measurements from a sample ranging between 1 and 41 ppm.

High-resolution transects of trace element concentrations were made across carbonate cements (Figure 5). The Holocene and Jurassic samples show an increase in the Mg/Ca ratios across the carbonate hardground cement, with a slower rate of change near the grain from which the cement nucleates and increasing Mg/Ca ratios along the growth axis (Figure 5a). In contrast, the modern and Triassic samples have no change in the Mg/Ca across the carbonate hardground cement (Figure 5b).

## 4. Discussion

Our samples were selected based on evidence of early lithification at the sediment/water interface through the presence of marine boring and encrusting organisms. In selecting the earliest cements and measuring multiple geochemical indicators, we hoped to test if carbonate hardground cements could be a viable medium for reconstructing seawater and/or early porewater chemistry. Sampling was focused on the earliest calcite cements, that is, syntaxial echinoderm overgrowths and fibrous cements when possible and, if not, the cements adjacent to primary grains (Figure 1). Initial diagenetic screening resulted in low Mn/Sr for most of our selected samples, suggesting they have neither gained much manganese nor lost much strontium, consistent with minimal diagenetic alternation (Table 4).

We will start with evaluating the modern sample to see if the calcite cement has a geochemistry reflective of the modern seawater. This sample, from the windward reef flat at Enewetak Atoll, was evaluated in detail by Carpenter et al. (1991). In that study, they found that the measured aragonite and calcite cements were in isotopic equilibrium with the ambient seawater. Additionally, they found that the system appeared to precipitate with minimal influence of kinetic effects based on the Sr-Mg relationship. In this study, we were able to confirm the isotopic values, adding $^{87}Sr/^{86}Sr$ values that are consistent with seawater. Additionally, the measured Ce anomaly is consistent with oxic deposition conditions. Finally, the measured Mg/Ca ratios calculate seawater with a Mg/Ca higher than measured, either a function of the samples being a high-Mg calcite, inaccuracies with the distribution coefficient, or enriched pore waters. Overall, this modern sample shows that in this environment and before diagenetic alteration, calcite cements are faithful recorders of seawater chemistry.

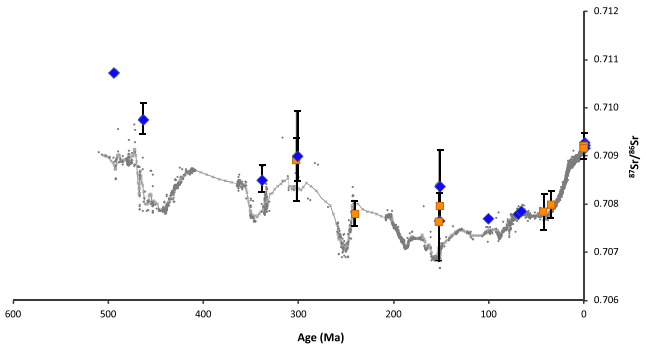


**Figure 4.** Seawater strontium $^{87}Sr/^{86}Sr$ record of Veizer et al. (1999) (green) with values from homogenized carbonate hardground cement fractions (red squares) and laser ablation (blue diamonds) in this study.

The remaining samples represent a range of primary environments, with a bias toward shallow, tidal environments. As listed in Table 1, all except for the Jurassic samples have tidal structures, consistent with shallow water and oxic environments. One caveat to the presumption of oxic tidal environments is evidence that early Paleozoic seas were not always oxic, even in shallow waters (Berner & Raiswell, 1983; Dahl et al., 2010; Sperling et al., 2015; Wallace et al., 2017). If so, the REYs are one tool for identifying anoxic environments. As such, the results from this study show no Ce anomaly.

Overall, each sample has some evidence of retaining a seawater signature. Many samples (Neogene, Oligocene, Triassic, and Carboniferous) have clear early cements as indicated by syntaxial echinoderm overgrowths and/or radiaxial fibrous calcite. Additionally, while many samples had later cementation phases, typically blocky pore-filling calcite (Eocene, Cretaceous, and Triassic), sampling could generally avoid these phases.

Geochemistry, Geophysics, Geosystems

10.1029/2019GC008448

**Table 4**
*Elemental Concentrations and Calculated Mg/Ca Seawater Ratio*

| | Age (Ma) | Stage | Period | Location | Number of sample points | Ave. Mn/Sr molar ratio | Ave. Sr conc. (ppm) | Ave. Mg conc. (wt %) | Ave. Mg/Ca molar ratio | 2 stand. error | Formational fluid Mg/Ca at 15 °C | 2 stand. error | Formational fluid Mg/Ca at 35 °C | 2 stand. error |
|---|---|---|---|---|---|---|---|---|---|---|---|---|---|---|
| 1 | 0 | Modern | Neogene | Enewetak Atoll, Marshalls Islands | 59 | 0.12 | 1,085 | 3.78 | 0.184 | 0.003 | 11.11 | 0.30 | 7.06 | 0.20 |
| 2 | 0.0007 | Late Holocene | Neogene | Intertidal Zone, Persian Gulf, UAE | 54 | 0.18 | 1,617 | 4.16 | 0.196 | 0.010 | 10.96 | 0.14 | 6.96 | 0.09 |
| 3 | 0.006 | Early Holocene | Neogene | Mussafah Channel Hardground, UAE | 16 | 0.07 | 1,250 | 3.88 | 0.213 | 0.020 | 10.45 | 1.62 | 6.64 | 1.03 |
| 4 | 35 | Lower Oligocene | Neogene | Suwannee Limestone, USA | 15 | 0.12 | 695 | 0.35 | 0.016 | 0.003 | 0.98 | 0.16 | 0.62 | 0.10 |
| 5 | 42 | Middle Eocene | Paleogene | Avon Park Formation, USA | 9 | 0.12 | 510 | 0.37 | 0.016 | 0.004 | 0.97 | 0.22 | 0.62 | 0.14 |
| 6 | 66 | Maastrichtian 1 | Cretaceous | Meerssen Member, the Netherlands | 7 | 0.20 | 650 | 0.57 | 0.020 | 0.008 | 1.53 | 0.37 | 0.97 | 0.23 |
| 7 | 125–129 | Aptian-Barremian | Cretaceous | Qishn Formation, Oman | 4 | 0.23 | 1,715 | 0.52 | 0.023 | 0.003 | 1.37 | 0.17 | 0.87 | 0.11 |
| 8 | 100 | Cenomanian | Cretaceous | Upper Greensands, Devon, UK | 15 | 0.79 | 502 | 0.57 | 0.022 | 0.003 | 1.13 | 0.04 | 0.72 | 0.03 |
| 9 | 145–161 | Valanginian | Jurassic | Gerecse Mts. of Hungary | 5 | 0.89 | 375 | 0.30 | 0.013 | 0.001 | 0.77 | 0.12 | 0.49 | 0.08 |
| 10 | 145–161 | Valanginian | Jurassic | Gerecse Mts. of Hungary | 4 | 0.98 | 466 | 0.50 | 0.023 | 0.002 | 1.40 | 0.03 | 0.89 | 0.16 |
| 11 | 242 | Triassic | Triassic | Latimar Formation | 4 | 0.43 | 405 | 0.11 | 0.004 | 0.003 | 0.27 | 0.15 | 0.17 | 0.10 |
| 12 | 299–305 | Kasimovian | Penn/Carb | Holder formation, New Mexico | 23 | 0.51 | 1,460 | 0.74 | 0.032 | 0.004 | 2.07 | 0.17 | 1.31 | 0.11 |
| 13 | 299–305 | Kasimovian | Penn/Carb | Holder formation, New Mexico | 11 | 1.15 | 1,097 | 0.79 | 0.043 | 0.008 | 2.61 | 0.50 | 1.66 | 0.31 |
| 14 | 331–347 | Visean | Carb | Eskett Limestones, England | 54 | 0.27 | 616 | 0.58 | 0.025 | 0.002 | 1.54 | 0.16 | 0.98 | 0.10 |
| 15 | 461–468 | Dariwillian | Ordovician | Kanosh Formation, Utah | 3 | 0.22 | 3,924 | 0.38 | 0.017 | 0.002 | 1.03 | 0.11 | 0.66 | 0.07 |
| 16 | 485–497 | Furongian | Cambrian 1 | Furongian, Banff National Park | 5 | 0.62 | 726 | 0.27 | 0.011 | 0.003 | 0.70 | 0.30 | 0.40 | 0.19 |
| 17 | 495–505 | Drumian | Cambrian 2 | Marjuman, Banff National Park | 3 | 0.96 | 650 | 0.38 | 0.017 | 0.010 | 1.03 | 0.58 | 0.65 | 0.37 |

No clear variations were found as a function of depositional environment, with the exception of the deeper water Jurassic sample and potential influences on $^{87}Sr/^{86}Sr$ from clays.

When evaluating evidence of significant diagenetic alteration, oxygen isotopes are readily reset and capture formation temperature, fluid $\delta^{18}O$, mineralogy, solution pH, and kinetic effects (Swart, 2015, and references herein). We note that, enigmatically, the oxygen isotope compositions of the carbonate hardground cements for the majority of samples are similar to the biogenic carbonate oxygen isotope curve, that is that they are lower in $\delta^{18}O$ going further back in time (Veizer et al., 1999). This is consistent with earlier studies of carbonate cements (Carpenter et al., 1991). The trend of lower $\delta^{18}O$ in carbonate minerals going back in time through the Phanerozoic is controversial and has been interpreted as either reflecting a change in the $\delta^{18}O$ of the ocean (such that early Phanerozoic oceans had a $\delta^{18}O$ that was −4‰ to −6‰ vs. 0‰ today) or to reflect diagenesis, such that the $\delta^{18}O$ of the carbonate minerals no longer has its initial $\delta^{18}O$ (Ryb & Eiler, 2018; Veizer et al., 1999). Changes to the $\delta^{18}O$ of carbonate minerals are largely a function of burial depth after deposition and degree to which the carbonate minerals have seen meteoric water, both fluids with a lower $\delta^{18}O$ than seawater. One challenge with explaining the $\delta^{18}O$ in carbonate mineral data being lower in the Paleozoic than the Mesozoic (Veizer et al., 1999). The carbonate hardground cements that we have chosen for this study were not buried to great depth as understood from the petrography and geological context of the samples (see references in Table 1 and section 4.1.1). However, we cannot rule out that the older hardgrounds have not seen more meteoric water or seen more late-stage diagenetic alteration than the younger hardgrounds, and older geological samples necessarily have more protracted histories than younger samples. The mechanism for this would be enigmatic. For the purpose of discussion, we will recognize that the drivers for $\delta^{18}O$ of the hardground cements may be more uncertain back in time.

For this discussion, we will use data to identify the features that may be influencing the geochemical composition of the carbonate hardground cement: first, whether and to what extent there is an influence of secondary fluids, either meteoric or burial; and second, how evolved from past seawater the carbonate hardground cements may be. We will consider each of these in turn.

### 4.1. Influence of Secondary Fluids on the Geochemistry of Carbonate Hardground Cements

#### 4.1.1. Influence of Meteoric Water

Many carbonate hardgrounds have at some point in their geological history, typically soon after lithification, have been subaerially exposed. During this subaerial exposure, they may be exposed to meteoric water, resulting in the recrystallization of carbonate mineral cements and/or new cements may precipitate in any remaining pore space. We note that two of our samples likely formed in deeper water and are less likely to have seen meteoric water (Samples 9 and 10 in Table 1). We will explore the extent of meteoric alteration of our carbonate hardground cements using the $^{87}Sr/^{86}Sr$ and the $\delta^{18}O$ of the carbonate minerals, as the $^{87}Sr/^{86}Sr$ and $\delta^{18}O$ of meteoric water consistently differ greatly from seawater.

The incorporation of radiogenic strontium ($^{87}Sr$) into carbonate minerals does not exhibit isotope fractionation. As such, the $^{87}Sr/^{86}Sr$ ratio in a carbonate mineral records the $^{87}Sr/^{86}Sr$ of the formational fluid and remains largely unchanged even if strontium is lost during mineral recrystallization (presuming no additional strontium incorporation). Furthermore, the $^{87}Sr/^{86}Sr$ composition of seawater is well constrained throughout the Phanerozoic (Veizer et al., 1999; Figure 4); thus, if our samples do not have the $^{87}Sr/^{86}Sr$ of the seawater curve, then either their age is incorrect or they have acquired $^{87}Sr/^{86}Sr$ from some later stage fluid. A third possibility is that the $^{87}Sr/^{86}Sr$ analysis suffers from contamination from clay minerals during sampling; however, we rule this out because we sampled using laser ablation with a 20 μm spot size, so we were able to avoid noncarbonate phases effectively, and the TIMS data agree with the laser ablation data.

Our samples fall close to the seawater $^{87}Sr/^{86}Sr$ curve for the last $100 \times 10^6$ years, while for the Jurassic, Devonian, and Cambrian, they fall distinctly above this curve (Figure 4). As meteoric water is nearly always more radiogenic than seawater (higher $^{87}Sr/^{86}Sr$), this suggests that these carbonate hardground cements may have exchanged strontium with meteoric water or other more radiogenic fluids. This does not preclude that they may retain some geochemical signature from seawater, but it is a point of concern. Ironically, the Jurassic sample is deposited in a succession of red marl interpreted to have formed in deeper water, where we would initially assume that influence from meteoric water would be less. It could be that for this sample, there was alteration of pore fluids from clay minerals, resulting in a more radiogenic $^{87}Sr/^{86}Sr$ value.

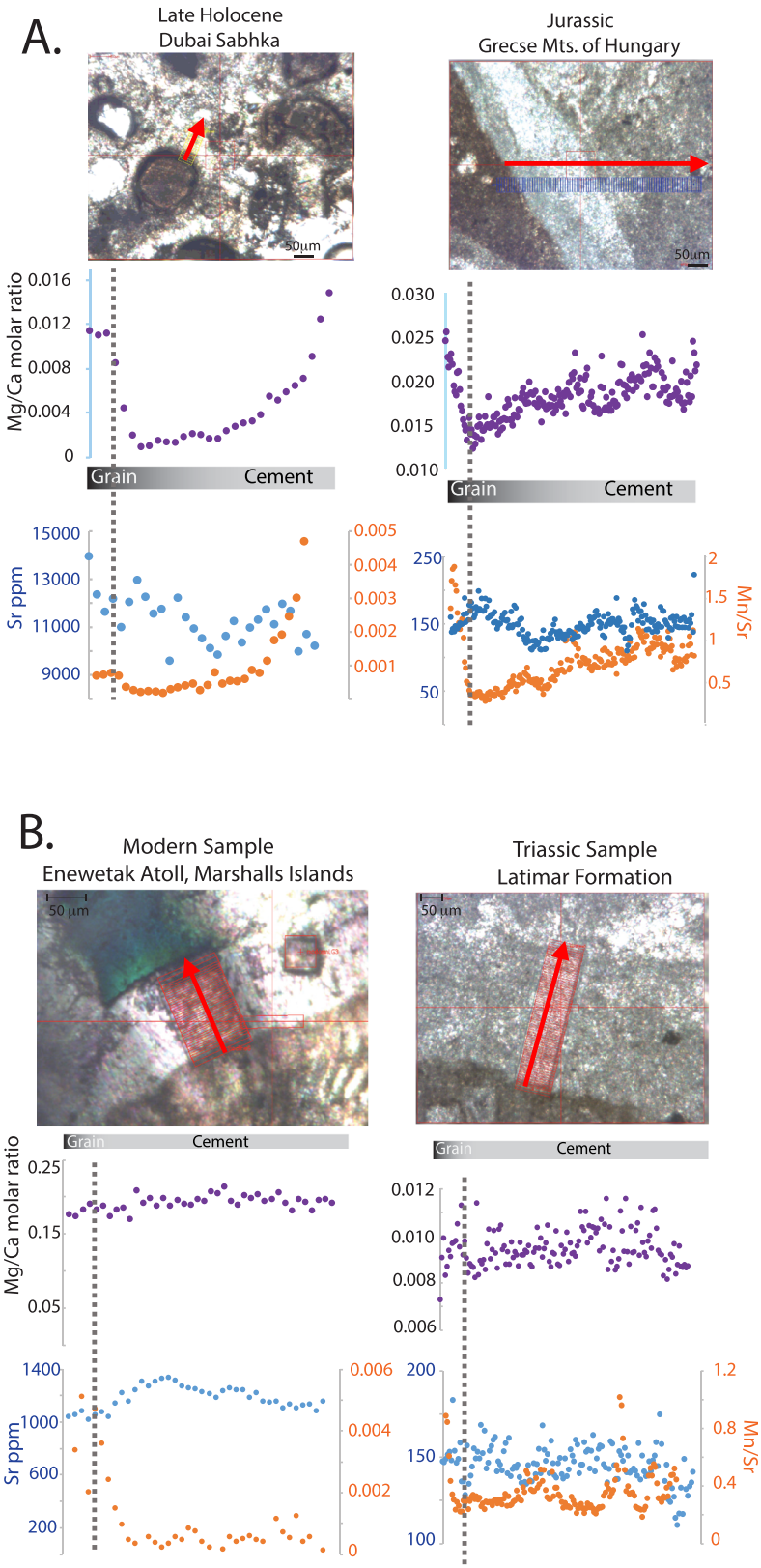


**Figure 5.** Mg/Ca ratios, strontium concentrations, and Mn/Sr ratios for samples showing examples of (a) closed and (b) open system precipitation behavior. Samples from potential closed system environments show an increase in Mg/Ca ratios along the growth axis, while samples from open systems show uniform Mg/Ca ratios. The red lines indicate the trace of the LA-ICPMS, and the grain boundary is denoted with a dashed gray line.

The $\delta^{18}O$ of the carbonate hardground cements in this study are similar to those measured in biogenic carbonates for samples in the Mesozoic and Cenozoic (approximately −2‰ to +1‰ $\delta^{18}O$; Veizer et al., 1999; Veizer & Prokoph, 2015). We note that the Early Holocene hardground has a higher $\delta^{18}O$, and higher Mg/Ca, than seawater which is consistent with deposition and/or alteration in an evaporative environment, corresponding to that sample being deposited a warm, dry region with high rates of evaporation. As mentioned above, our samples from the Paleozoic have far more negative $\delta^{18}O$, that is, values less than −4‰. When these low $\delta^{18}O$ are coupled with higher-than-seawater $^{87}Sr/^{86}Sr$, it could be that the carbonate hardground cements may have interacted with meteoric water, which is lower in $\delta^{18}O$, at some point after formation.

We suggest that our Paleozoic samples appear to have been influenced by meteoric water given the high $^{87}Sr/^{86}Sr$ and low $\delta^{18}O$, while the samples younger than 100 Ma look more similar to primary seawater precipitates, which have seen less meteoric water. As discussed above, it is possible that the older carbonate hardgrounds have experienced more protracted burial histories; however, existing data suggest that the samples we have chosen were minimally buried. What is interesting is the samples from the Mesozoic, which either fall off the $^{87}Sr/^{86}Sr$ seawater curve but have a seawater-consistent $\delta^{18}O$ (the Jurassic) or fall on the $^{87}Sr/^{86}Sr$ seawater curve but have a distinctly negative $\delta^{18}O$ (the Triassic). These scenarios can result from reprecipitation at a time with a higher $^{87}Sr/^{86}Sr$ seawater but seawater-like temperatures or secondary alteration during burial, increasing the temperature but not significantly changing the pore water chemistry.

#### 4.1.2. Influence of Burial Fluids

As burial diagenesis can overprint primary mineralogy and chemistry, we need to either establish that burial, and burial fluid influence, was minimal and/or determine what impact burial fluids had on this system. While precise burial depths and temperature profiles were not available for most samples and their construction were outside the scope of this study, a review of previous studies can provide general bounds for diagenetic conditions. Overall, samples generally only experienced shallow burial, with the exception of two samples, the Triassic and the Ordovician samples.

The first, the Triassic Latemar formation, consists of multiple cement stages likely representing successive diagenetic phases (Christ et al., 2012). Christ et al. (2012) measured each of these phases, finding that while the radiaxial fibrous calcite had $\delta^{18}O$ values similar to projected seawater $\delta^{18}O$, the blocky, pore-filling calcite had very negative $\delta^{18}O$ values. These negative values were interpreted to reflect a deep burial domain, not meteoric diagenesis, based on the cement morphology. As a result, only the early calcite cements were used in this study. Additionally, the measurements of the $^{87}Sr/^{86}Sr$ of these cements via laser ablation fall on the established seawater strontium curve for this time, supporting these cements as relatively unaltered by burial fluids.

Additionally, the Ordovician sample may have experienced deeper burial. Using conodont alteration indices in carbonate interbeds, a burial temperature range between 60 and 450 °C was proposed (McDowell, 1995). While this range is large, it supports burial influence on this sample. This sample had the highest average strontium concentration of all the samples measured, along with a more radiogenic $^{87}Sr/^{86}Sr$ value (0.70978 vs. seawater at ~0.7085), consistent with burial alteration. The relatively negative $\delta^{18}O$ values from this sample may also represent the influence of burial fluids. As such, this sample should be evaluated with caution when considering potential seawater reconstructions.

The oldest samples in the study, that is, the Cambrian, have a more localized secondary fluid diagenesis. As these rocks have been uplifted as part of the Canadian Rockies, there is ample opportunity for the incursion of chemically altering fluids. These fluids appear to be limited to regions adjacent to faults (Aitken, 1978). While some of the adjacent formations are at least partially dolomitized, Aitken (1978) finds little evidence for deep burial. In this study, these samples had the most negative $\delta^{18}O$ values measured, along with radiogenic $^{87}Sr/^{86}Sr$ values. While these samples may have avoided deep burial, they do not appear to reflect established seawater values for the Cambrian.

The remainder of the samples was either Quaternary and had no opportunity for burial or previous authors have found little evidence of deep burial. Samples either preserved delicate, primary plant structures (Maastrichtian, Van der Ham et al., 2007); maintained syntaxial echinoderm overgrowths with only

shallow proposed burial depths (Oligocene/Eocene, Budd, 2002); or proposed temperatures that were inconsistent with hot diagenetic processes in a deep burial environment (Jurassic; Jenkyns & Clayton, 1986). These results are consistent with the relatively positive $\delta^{18}O$ values measured in this and other studies.

### 4.2. How Evolved From Seawater Is the Fluid From Which the Cements Precipitated?

All of the carbonate hardgrounds used in our study originally formed in likely oxygenated waters near the sediment-water interface; only the two Jurassic samples were from deeper depths but still on the slope, so possibly up to a few hundred meters water depth. Ocean anoxia during the earliest Phanerozoic may have extended into shallower water depths (Berner & Raiswell, 1983; Dahl et al., 2010; Sperling et al., 2015; Wallace et al., 2017), further complicating depositional reconstructions. This does not mean that all our hardgrounds would have formed in water that looks like bulk ocean water chemistry; in restricted or semi-restricted shallow platforms where carbonate hardgrounds may form, there can be a chemical evolution from the global ocean, meaning restricted platform settings may not have the same $\delta^{18}O$ or major ion chemistry as the global ocean (Lowenstein et al., 2003). Many chemical changes occur within sedimentary pore fluids as they are buried below the sediment-water interface. Many of these have to do with the fact that oxygen penetration into sediments is limited, controlled by diffusion and the constant consumption through respiration. The lack of oxygen can help with carbonate mineral precipitation and cementation, as anaerobic respiration tends to increase pH and the removal of sulfate is a key kinetic inhibitor to carbonate precipitation (Fernández-Díaz et al., 2010).

If we wish to understand how much the geochemistry of carbonate hardground cements represents pore fluid or seawater, one approach would be to look for geochemical signals that indicate oxic or anoxic conditions, since those that are notably anoxic would be a strong sign that the fluid was evolved within a sedimentary system away from the overlying water or that the overlying water was not oxygenated. One way to explore the oxic versus anoxic characteristics of the pore fluids is through the use of Ce anomalies. The presence of a characteristic seawater REY patterns, namely, a negative Ce anomaly and a positive Y anomaly, has been used as evidence that carbonate minerals precipitated in oxic, seawater conditions (Elderfield, 1988; German & Elderfield, 1990). Pore fluids often have higher concentrations of REYs and a Ce anomaly, though this is dependent on the redox state of the pore fluids (Deng et al., 2017; Haley et al., 2004). The concentration of REYs may increase due to anoxic fluids and the general reductive mobilization of metals. Carbonate minerals with no or slightly positive Ce anomaly may have precipitated in anoxic waters (Wallace et al., 2017), while negative anomalies are consistent with oxidizing conditions (Tostevin et al., 2016). The Ce anomaly has been suggested to be relatively robust to diagenetic alteration, even during polymorph recrystallization (cf. Wallace et al., 2017).

Unfortunately, Ce anomalies cannot be unambiguously interpreted, there can be multiple interpretations from a positive or flat Ce anomaly, making this tool indicative but not definitive. For example, Tostevin et al. (2016) measured carbonate ooze and deep-water carbonates from anoxic environments which had slightly positive Ce anomalies, while the carbonate cement precipitated in definitively anoxic conditions had no Ce anomaly. Similarly, a recent study of modern ooids from the Bahama Banks has a positive Ce anomaly, although they clearly precipitated from oxic water; the authors interpreted this as precipitation in highly alkaline conditions (Li et al., 2019). Therefore, while a positive or flat Ce anomaly may have several interpretations, it is rare that observation of a negative Ce anomaly is not interpreted as evidence for precipitation from oxic waters (Wallace et al., 2017). For this study, five samples had negative Ce anomalies, the modern sample from Enewetak Atoll, Oligocene 1, Jurassic 1, the Permian, and Pennsylvanian samples, hinting at precipitation from oxic fluids.

Total REY concentrations cannot be calculated as not all REEs were measured. The range of average normalized concentrations, spanning 1 to 0.0001, is large though not significantly outside the ranges observed in other studies (Hu et al., 2014; Jiang et al., 2015; Tostevin et al., 2016; Zhao & Zheng, 2017). Higher REY concentrations may result from our use of a laser ablation system, preventing the limited recovery observed with incomplete bulk dissolution (Tostevin et al., 2016). In our samples, the lowest REY concentrations are found within the modern Enewetak sample, consistent with the hypothesis of increased incorporation of REYs over time through pore fluid precipitation with higher overall concentrations of REEs in the pore fluids.

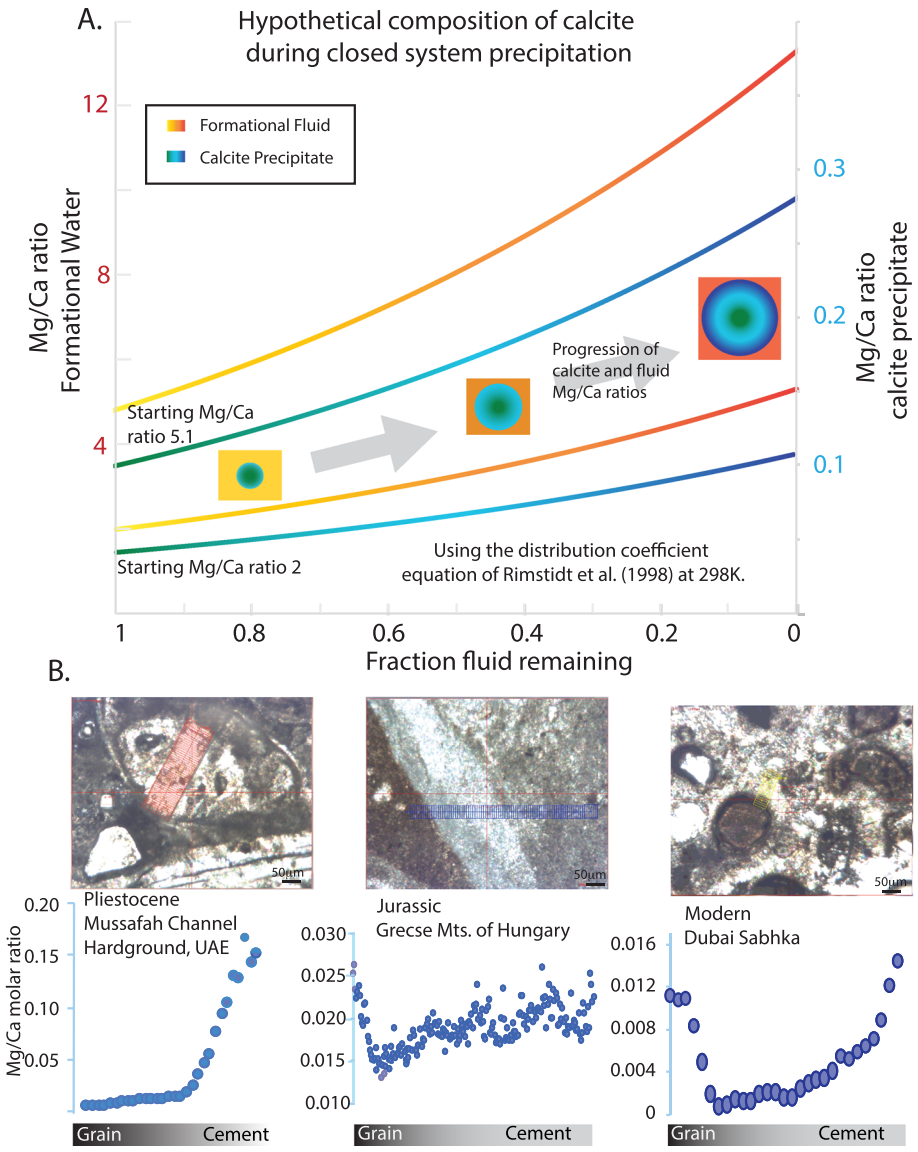


**Figure 6.** (a) Idealized model of pore water and calcite Mg/Ca ratios during calcite precipitation in a closed system. The evolution of pore water and the corresponding precipitate are shown for two starting Mg/Ca ratios and utilizing the distribution coefficient equation of Rimstidt et al. (1998) at 298 K. In both scenarios, successive precipitation of calcite corresponds to an increase in Mg/Ca ratios from the nucleation point to the most recent precipitate. (b) Idealized model of pore water calcite in an open system. Here, due to the constant fluid composition, calcite precipitates maintain a constant Mg/Ca ratio.

We can couple these results from REY data, which we suggest flags the influence of pore fluids (with the caveat that Ce anomalies can be equivocal on the redox conditions of precipitation) with carbon isotopes measured in the carbonate hardground cements. Carbon isotopes in carbonate minerals have minimal carbon isotope fractionation from the fluid from which they precipitate. The carbon isotopic composition of the global ocean over the Phanerozoic ranged from 0‰ to +5‰ (Veizer et al., 1999). The carbon isotope composition of the dissolved inorganic carbon in sedimentary pore waters tends to decrease, as the oxidation of organic carbon (which is more $^{12}C$ enriched) generates dissolved inorganic carbon that is lower in $\delta^{13}C$ (Sivan et al., 2007). Therefore, carbonate minerals that have lower $\delta^{13}C$ may reflect precipitation in evolved pore fluid subject to oxidation of organic carbon (e.g., Schrag et al., 2013). Often, the $\delta^{13}C$ is used in conjunction with the $\delta^{18}O$ to highlight postdepositional diagenesis, such as using more negative $\delta^{13}C$ and $\delta^{18}O$ as indicators for the influence of meteoric water or deep burial diagenesis.

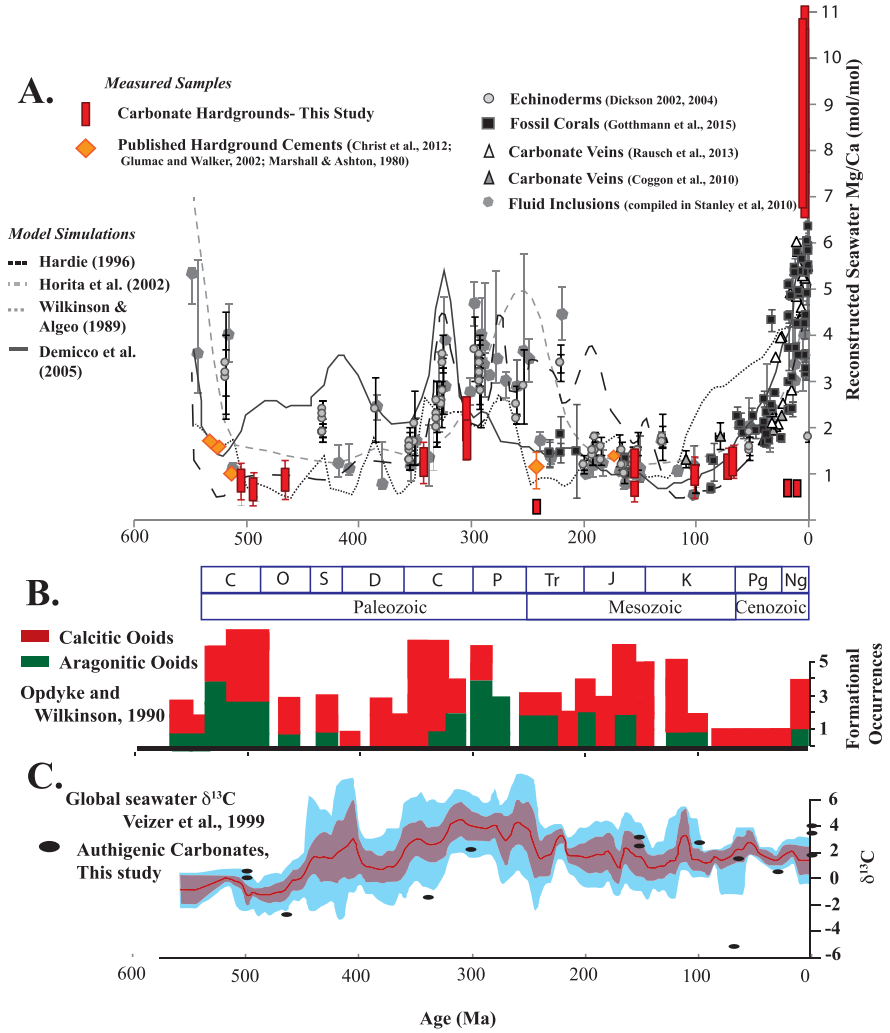


**Figure 7.** (a) Compilation of reconstructions of Mg/Ca ratios throughout the Phanerozoic. Results from this study are shown as red bars, with the range representing the range of possible seawater temperature (15–35 °C). Values from this study represent an upper limit for Mg/Ca ratios. (b) Occurrences of aragonitic versus calcitic ooids have been used to infer the predominant carbonate mineral precipitated during the Phanerozoic. (c) Global seawater $\delta^{13}C$ record of Veizer et al. (1999) with $\delta^{13}C$ of carbonate hardground cements from this study.

Our measured $\delta^{13}C$ fall largely in the range expected from seawater over the Phanerozoic. We note one sample that has a highly negative $\delta^{13}C$ (−5‰) but interestingly does not have a very negative $\delta^{18}O$. We suggest that this sample may have precipitated from evolved pore fluids that had organic matter respiration but no change in the oxygen isotope composition.

As neither the use of REY nor $\delta^{13}C$ can unambiguously define precipitation in evolved pore water versus in seawater, we can use our data from laser ablation and/or electron microprobe to provide information on changing concentrations at the micron scale during growth of the carbonate hardground cement. The principle of this can be illustrated with a simple example based on Rayleigh distillation. If we consider the case of magnesium incorporation into carbonate minerals, the first precipitates will take in more calcium than magnesium from the formational fluid as illustrated by the partition coefficients developed by Rimstidt et al. (1998) among others. This results in more magnesium remaining in the fluid relative to calcium, increasing the Mg/Ca ratio of the fluid. The next stage of mineral precipitation takes place in a slightly higher Mg/Ca ratio fluid, which is then reflected in the next mineral precipitate. If taken to the extreme, the Mg/Ca ratio of the fluid, and therefore the precipitate, can triple through this process in a strictly closed system (Figure 6a). The opposite trend in Mg/Ca ratios occurs during carbonate dissolution. Since carbonate minerals have

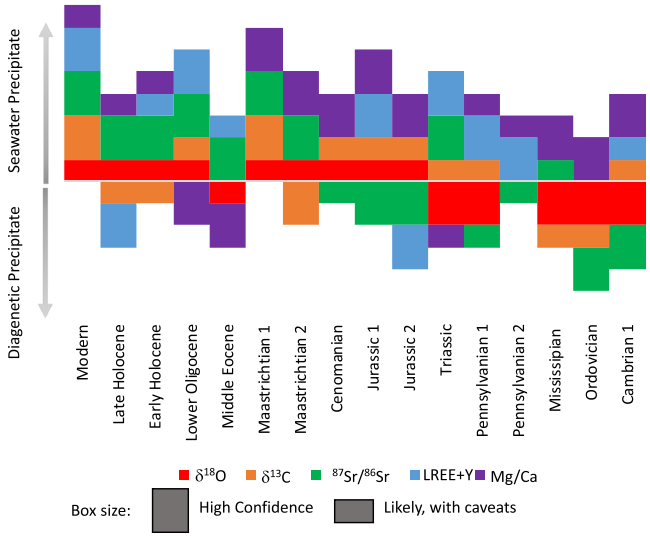


**Figure 8.** Conceptual representation of the confidence of each variable to represent precipitates in equilibrium with seawater or diagenetically altered carbonate. The confidence was defined as follows: (1) a high confidence when was assigned when the geochemical measurement was consistent with predicted values, (2) likely with caveats for samples that were within the probable range for the proposed time period, (3) negatively likely with caveats for samples that are outside the probable range for seawater precipitates though not clearly diagenetic, and (4) negatively high confidence for samples showing clear diagenetic indicators.

lower Mg/Ca ratios than pore fluids, the dissolution of carbonate minerals has the potential to lower the fluid Mg/Ca. Both increases and decreases in pore fluid Mg/Ca are observed in modern pore water profiles, implying regions of both precipitation and dissolution of carbonate minerals within modern sedimentary systems (Sun et al., 2016).

In theory, measuring a transect, if there is an evolution in a trace element ratio or concentration, allows us to identify and measure the earliest carbonate cement precipitate and reconstruct the pore fluid evolution during cement formation. Some sedimentary environments, particularly those that are near the sediment-water interface, may behave more as an open system with contact with overlying seawater where fluid is continually introduced through advection. Increases in wave and current strength result in higher rates of circulation within the uppermost sediments, providing a steady influx of calcium and carbonate ions possibly helping promote carbonate precipitation (Christ et al., 2015; Coimbra et al., 2009). This regular exchange with seawater results in pore water chemistry that is constant and remains similar to that of the overlying seawater. As a result, the composition of the precipitating calcite remains constant (Figure 6b). These high water-rock ratios that promote "open-system" conditions may lead to both flat Mg/Ca and a flattening of the REY profiles (Perry et al., 1976; Zhao & Zheng, 2017). Future studies where these geochemical parameters (both Mg/Ca and REY) are measured on the same transect could test this hypothesis.

In our transects across the carbonate hardground cements, we see a mixture of this closed and open system behavior (Figure 5). The modern and Triassic samples show constant Mg/Ca ratios along the growth axis, while the Late Holocene and Jurassic samples show increases in the Mg/Ca ratio along the calcite growth axis (Figure 5). These changes could be the result of closed system precipitation in pore fluid that is chemically evolving.

### 4.3. Reconstructing Formational Mg/Ca for the Carbonate Hardground Cements

When the measured Mg/Ca ratios are translated into formational fluid using the Mg/Ca distribution coefficient of Rimstidt et al. (1998), we note lower formational fluid Mg/Ca for all time periods apart from the modern (Figure 7). We note that our carbonate hardgrounds from the modern have a higher reconstructed Mg/Ca than the known modern ocean. This could be because of precipitation in a restricted or mildly evaporitic location, where initial calcite precipitation has driven the Mg/Ca of the fluid higher or the fact that many of these will have precipitated as high-Mg calcite and therefore the equation used for the partition coefficient yields higher Mg concentrations in the formational fluid. Our reconstructed Mg/Ca for the rest of the Phanerozoic is not inconsistent with other proxies for seawater Mg/Ca (Figure 7), although we do note that we are missing high Mg/Ca for the latest part of the Paleozoic when other proxies suggest there is high seawater Mg/Ca. A complicating factor for the reconstruction of Mg/Ca using carbonate hardground cements during oceans with high Mg/Ca is that the dominant carbonate cement that precipitate in a high Mg/Ca fluid will be high-Mg calcite, which is less stable and will transform to calcite, losing some Mg on the way, and will not retain its same Mg/Ca (Bischoff et al., 1993). The fact that different carbonate polymorphs tend to precipitate in oceans with different major ion chemistry and that different calcium carbonate polymorphs have different distribution coefficients makes unravelling this trickier. This can be circumvented if the mineral precipitate has not changed over time (e.g., echinoderm fragments, Dickson, 2002, 2004; aragonitic corals, Gothmann et al., 2015; calcite in veins, Coggon et al., 2010, Rausch et al., 2013). For this study, there is also a notable lack of carbonate hardgrounds during times of high Mg/Ca in the late Paleozoic (Christ et al., 2015).

Here, only the samples that preserved a high seawater Mg/Ca ratio in their earliest preserved precipitates were Holocene or younger in age (Figure 7). These samples likely did not have time to undergo recrystallization to low-Mg calcite, and thus, the magnesium concentration in the measured carbonate hardground cement is high. Indeed, visual inspection of Holocene thin sections shows larger pore spaces and little

evidence of compaction. The Oligocene and Eocene samples, while also forming during a time with a likely relatively high Mg/Ca seawater, do not retain the enhanced Mg/Ca ratios that would be reflective of primary precipitation and a direct recorder of seawater. While a transformation from high to low-Mg calcite was not clear on petrographic images, the $\delta^{18}O$ of the Eocene sample was inconsistent with direct seawater precipitation, implying some secondary alteration. The results from this study do show reconstructed Mg/Ca seawater ratios from carbonate hardgrounds falling within accepted ranges during periods of predicted lower seawater Mg/Ca ratios. As shown in Figure 7, samples from the Cretaceous, Jurassic, Carboniferous, Ordovician, and Cambrian were consistent with values predicted from other studies.

## 5. Summary

The main objective of this work was to see if the cements in carbonate hardgrounds provide insight into early pore water conditions and, by extension, if they can be used as an archive of seawater chemistry. While pore waters near the sediment-water interface may preserve the $^{87}Sr/^{86}Sr$ and $\delta^{18}O$ of seawater, these fluids can be geochemically altered in other ways. In these instances, $\delta^{13}C$ of precipitated carbonate hardground cements can indicate the interaction with dissolved inorganic carbon derived from the oxidation of organic carbon, while REY results can further denote anoxic conditions. Finally, reprecipitation can be captured by monitoring of Mn/Sr and absolute strontium concentrations.

Using this multiproxy evaluation tool, most of the carbonate hardground samples in this study had some indication of secondary alteration and/or formation in waters not in equilibrium with seawater or with what we think seawater should have been. The modern sample, presumed to be unaltered, was the only sample to meet all the criteria suggesting it retained a primary seawater signal. Even though the remainder of the samples did not fully pass the thresholds outlined, by analyzing a larger suite of proxies, it is possible to constrain when alteration occurred (Figure 8).

Although two samples from the Holocene had $^{87}Sr/^{86}Sr$ ratios consistent with precipitation from primary seawater, further geochemical evidence support formation from evolved porewaters. Neither sample had a negative Ce anomaly, and the $\delta^{18}O$ was inconsistent with Holocene seawater. Additionally, the Mg/Ca ratio is higher than predicted, consistent with closed system precipitation. As these samples have not been extensively buried, they provide evidence that cements from carbonate hardgrounds are forming rapidly in closed systems that show varying degrees of pore water alteration.

A second set of samples, those from the Oligocene and Eocene, shows a different assemblage of results. In these samples, $^{87}Sr/^{86}Sr$ ratios, $\delta^{18}O$, and the negative to flat Ce anomalies support precipitation from seawater. However, the Mg/Ca are significantly lower than established records. These results are consistent with reprecipitation from high-Mg calcite to low-Mg calcite occurring in a closed system, preserving original Sr and limiting the changes in REY while maintaining the same temperature conditions.

Older samples, that is, the remaining Cenozoic and Paleozoic samples, showed further deviation from seawater. While all the samples preserved Mg/Ca ratios consistent with published records, only some samples preserved contemporary $^{87}Sr/^{86}Sr$ ratios, and the Palaeozoic samples did not have $\delta^{18}O$ values in line with the generally accepted values for seawater. Additionally, the REY results were inconclusive for these samples, underlining the difficulty in preserving primary signals while highlighting the need for the analysis of multiple geochemical records.

We suggest that carbonate hardground cements may be a useful tool for looking at past environmental and oceanographic changes but that multiple geochemical proxies must be used to tease apart the various constraints. What remains enigmatic in studies of Phanerozoic paleoceanography is the fact that across multiple geochemical proxies and in many different mineral phases, samples that are older are systematically more altered than samples that are younger. Carbonate hardground cements with detailed petrography should be useful as rapid cementation means chemical compositions are fixed early, and only deep burial diagenesis may alter these chemical signals. However, it remains unclear the influence of initial carbonate polymorph and how these changes early in diagenesis influence the concentrations that are measured within the cements. Future work linking petrographically focused studies with detailed geochemical analyses will help clarify these connections.

## Data Statement

Data are archived in the PANGAEA data repository (https://doi.pangaea.de/10.1594/PANGAEA.910001).

**Acknowledgments**
We gratefully thank David Budd, Orsolya Győri, Brian Pratt, and Stephen Lokier for providing samples for this study, James Rolfe for assistance with carbon and oxygen isotopic measurements, Peter Scott for assistance with laser-ablation strontium isotopes, and Harold Bradbury for assistance with TIMS. This manuscript has been greatly improved though the constructive feedback of Ashleigh Hood and two anonymous reviewers. Funding for this project was provided by the Canadian Institute for Advanced Research (CIFAR) to A. M. E. and ERC StG Grant 307582 (CARBONSINK) to A. V. T.

## References

Ahm, A.-S. C., Bjerrum, C. J., Blättler, C. L., Swart, P. K., & Higgins, J. A. (2018). Quantifying early marine diagenesis in shallow-water carbonate sediments. *Geochimica et Cosmochimica Acta*, *236*, 140–159.

Aitken, J. D. (1978). Revised models for depositional grand cycles, Cambrian of the southern Rocky Mountains, Canada. *Bulletin of Canadian Petroleum Geology*, *26*, 515.

Bau, M., & Dulski, P. (1996). Distribution of yttrium and rare-earth elements in the Penge and Kuruman iron-formations, Transvaal Supergroup, South Africa. *Precambrian Research*, *79*, 37–55.

Berner, R. A., & Raiswell, R. (1983). Burial of organic carbon and pyrite sulfur in sediment over phanerozoic time: A new theory. *Geochimica et Cosmochimica Acta*, *47*, 855–862.

Bischoff, W. D., Bertram, M. A., Mackenzie, F. T., & Bishop, F. C. (1993). Diagenetic stabilization pathways of magnesian calcites. *Carbonates and Evaporites*, *8*, 82–89.

Brand, U., & Veizer, J. (1980). Chemical diagenesis of a multicomponent carbonate system; 1, trace elements. *Journal of Sedimentary Research*, *50*, 1219–1236.

Bromley, R. G. (1978). Hardground diagenesis. In R. W. Fairbridge & J. Bourgeois (Eds.), *The encyclopedia of sedimentology* (pp. 397–400). Stroudsburg, Pennsylvania: Dowden, Hutchinson & Ross.

Budd, D. A. (2002). The relative roles of compaction and early cementation in the destruction of permeability in carbonate grainstones: A case study from the Paleogene of west-central Florida, USA. *Journal of Sedimentary Research*, *72*, 116–128.

Burton, E. A., & Walter, L. M. (1991). The effects of $PCO_2$ and temperature on magnesium incorporation in calcite in seawater and $MgCl_2$-$CaCl_2$ solutions. *Geochimica et Cosmochimica Acta*, *55*, 777–785.

Carpenter, S. J., Lohmann, K. C., Holden, P., Walter, L. M., Huston, T. J., & Halliday, A. N. (1991). $\delta^{18}O$ values, $^{87}Sr/^{86}Sr$ and Sr/Mg ratios of Late Devonian abiotic marine calcite: Implications for the composition of ancient seawater. *Geochimica et Cosmochimica Acta*, *55*, 1991–2010.

Christ, N., Immenauser, A., Wood, R. A., Darwich, K., & Niedermayr, A. (2015). Petrography and environmental controls on the formation of Phanerozoic marine carbonate hardgrounds. *Earth-Science Reviews*, *15*, 176–226.

Christ, N., Immenhauser, A., Amour, F., Mutti, M., Preston, R., Whitaker, F. F., et al. (2012). Triassic latemar cycle tops—Subaerial exposure of platform carbonates under tropical arid climate. *Sedimentary Geology*, *265-266*, 1–29.

Christensen, J. N., Halliday, A. N., Lee, D.-C., & Hall, C. M. (1995). In situ Sr isotopic analysis by laser ablation. *Earth and Planetary Science Letters*, *136*, 79–85.

Coggon, R. M., Teagle, D. A. H., Smith-Duque, C. E., Alt, J. C., & Cooper, M. J. (2010). Reconstructing past seawater Mg/Ca and Sr/Ca from mid-ocean ridge flank calcium carbonate veins. *Science*, *327*, 1114–1117.

Coimbra, R., Immenhauser, A., & Olóriz, F. (2009). Matrix micrite $\delta^{13}C$ and $\delta^{18}O$ reveals synsedimentary marine lithification in Upper Jurassic Ammonitico Rosso limestones. *Sedimentary Geology*, *219*, 332–348.

Cummins, R. C., Finnegan, S., Fike, D. A., Eiler, J. M., & Fischer, W. W. (2014). Carbonate clumped isotope constraints on Silurian ocean temperature and seawater $\delta^{18}O$. *Geochimica et Cosmochimica Acta*, *140*, 241–258.

Dahl, T. W., Hammarlund, E. U., Anbar, A. D., Bond, D. P. G., Gill, B. C., Gordon, G. W., et al. (2010). Devonian rise in atmospheric oxygen correlated to the radiations of terrestrial plants and large predatory fish. *Proceedings of the National Academy of Sciences*, *107*, 17,911–17,915.

Dean, M. T., Browne, M. A. E., Waters, C. N., & Powell, J. H. (2011). A lithostratigraphical framework for the Carboniferous successions of northern Great Britain (onshore). British Geological Survey, 165 pp.

Deng, Y., Ren, J., Buo, Q., Cau, J., Wang, H., & Liu, C. (2017). Rare earth element geochemistry characteristics of seawater and porewater from deep sea in western Pacific. *Scientific Reports*, *7*(1), 1, 16539–13.

Derry, L. A., Kaufman, A. J., & Jacobsen, S. B. (1992). Sedimentary cycling and environmental change in the Late Proterozoic: Evidence from stable and radiogenic isotopes. *Geochimica et Cosmochimica Acta*, *56*, 1317–1329.

Dickson, J. A. D. (2002). Fossil echinoderms as monitor of the Mg/Ca ratio of Phanerozoic Oceans. *Science*, *298*(5596), 1222–1224. https://doi.org/10.1126/science.1075882

Dickson, J. A. D. (2004). Echinoderm skeletal preservation: Calcite-aragonite seas and the Mg/Ca ratio of the Phanerozoic oceans. *Journal of Sedimentary Research*, *74*, 355–365.

Dickson, J. A. D., Wood, R. A., Bu Al Rougha, H., & Shebl, H. (2008). Sulphate reduction associated with hardgrounds: Lithification afterburn! *Sedimentary Geology*, *205*, 34–39.

Dravis, J. (1979). Rapid and widespread generation of recent oolitic hardgrounds on a high energy Bahamian platform, Eleuthera bank, Bahamas. *Journal of Sedimentary Petrology*, *49*, 195–207.

Dupraz, C. R., Reid, R. P., Braissant, O., Decho, A. W., Norman, R. S., & Visscher, P. T. (2009). Processes of carbonate precipitation in modern microbial mats. *Earth-Science Reviews*, *96*(3), 141–162. https://doi.org/10.1016/j.earscirev.2008.10.005

Elderfield, H. (1988). The oceanic chemistry of the rare-earth elements. *Philosophical Transactions of the Royal Society A*, *325*, 105–126.

Emrich, K., Ehhalt, D. H., & Vogel, J. C. (1970). Carbon isotope fractionation during the precipitation of calcium carbonate. *Earth and Planetary Science Letters*, *8*, 363–371.

Fernández-Díaz, L., Fernández-González, Á., & Prieto, M. (2010). The role of sulfate groups in controlling $CaCO_3$ polymorphism. *Geochimica et Cosmochimica Acta*, *74*, 6064–6076.

Fike, D. A., Bradley, A. S., & Rose, C. (2015). Rethinking the ancient sulfur cycle. *Annual Reviews of Earth and Planetary Science*, *43*, 593–622.

Friedman, I., & O'Neil, J. R. (1977). Compilation of stable isotope fractionation: Factors of geochemical interest. In M. Fleischer (Ed.), *Data of geochemistry*, *Geol. Surv. Prof. Paper, KK* (6th ed., pp. 1–12). Washington, DC: USGS.

Fursich, F. T., Oschmann, W., Singh, I. B., & Jaitly, A. K. (1992). Hardgrounds, reworked concretion levels, and condensed horizons in the Jurassic of western India: Their significance for basin analysis. *Journal of the Geological Society*, *149*, 313–331.

Gabitov, R. I., Sadekov, A., & Migdisov, A. (2017). REE incorporation into calcite individual crystals at one time spike addition. *Minerals*, *7*, 204.

Gallois, R. (2005). The stratigraphy of the Upper Greensand (Cretaceous) of south-west England. *Geoscience in south-west England*, *11*, 21–29.
German, C. R., & Elderfield, H. (1990). Application of the Ce anomaly as a paleoredox indicator: The ground rules. *Paleoceanography*, *5*, 823–833.
Givan, R. K., & Lohmann, K. C. (1985). Spatial and temporal controls on the variation of original isotopic compositions of Permian marine carbonates. *Journal of Sedimentary Petrology*, *55*, 430–439.
Goldstein, R. H. (1988). Cement stratigraphy of Pennsylvanian Holder Formation, Sacramento Mountains, New Mexico. *AAPG Bulletin*, *72*(4), 425–438.
Gothmann, A. M., Stolarski, J., Adkins, J. F., Schoene, B., Dennis, K. J., Schrag, D. P., et al. (2015). Fossil corals as an archive of secular variations in seawater chemistry since the Mesozoic. *Geochimica et Cosmochimica Acta*, *160*, 188–208.
Haley, B. A., Klinkhammer, G. P., & McManus, J. (2004). Rare earth elements in pore waters of marine sediments. *Geochimica et Cosmochimica Acta*, *68*, 1265–1279.
Hu, Y., Feng, D., Peckmann, J., Roberts, H. H., & Dhen, D. (2014). New insights into cerium anomalies and mechanisms of trace metal enrichment in authigenic carbonate from hydrocarbon seeps. *Chemical Geology*, *381*, 55–66.
Immenhauser, A., Immenhauser, A., Hillgärtner, H., Sattler, U., Bertotti, G., Schoepfer, P., et al. (2004). Barremian-lower Aptian Qishn Formation, Haushi-Huqf area, Oman: A new outcrop analogue for the Kharaib/Shu'aiba reservoirs. *GeoArabia*, *9*, 153–194.
Jenkyns, H. C., & Clayton, C. J. (1986). Black Shales and carbon isotopes in pelagic sediments from the Tethyan Lower Jurassic. *Sedimentology*, *33*, 87–106.
Jiang, L., Cai, C., Worder, R. H., Li, K., Xiang, L., Chu, X., et al. (2015). Rare earth element and yttrium (REY) geochemistry in carbonate reservoirs during deep burial diagenesis: Implications for REY mobility during thermochemical sulfate reduction. *Chemical Geology*, *415*, 87–101.
Kennedy, W. J., & Garrison, R. E. (1975). Morphology and genesis of nodular chalks and hardgrounds in the Upper Cretaceous of southern England. *Sedimentology*, *22*, 311–386.
Khalaf, F., Milliman, J. D., & Druffel, E. M. (1987). Submarine limestones in the nearshore environment off Kuwait, northern Arabian Gulf. *Sedimentology*, *34*, 67–75.
Lawrence, M. G., Greig, A., Collerson, K. D., & Kamber, B. S. (2006). Rare Earth Element and Yttrium variability in South East Queensland waterways. *Aquatic Geochemistry*, *12*, 39–72. https://doi.org/10.1007/s10498-005-4471-8
Li, F., Webb, G. E., Algeo, T. J., Kershaw, S., Lu, C., Oehlert, A. M., et al. (2019). Modern carbonate ooids preserve ambient aqueous REE signatures. *Geochimica et Cosmochimica Acta*, *509*, 163–177.
Lighty, R. G. (1985). Preservation of internal reef porosity and diagenetic sealing of submerged early Holocene Barrier Reef, SE Florida Shelf. *Carbonate Cements*, *SEPM*, SP36, 123–151.
Lohmann, K. C., & Walker, J. C. G. (1989). The $\delta^{18}O$ record of Phanerozoic abiotic marine calcite cements. *Geophysical Research Letters*, *16*, 319–322.
Lorens, R. (1981). Sr, Cd, Mn and Co distribution coefficients in calcite as a function of calcite precipitation rate. *Geochimica et Cosmochimica Acta*, *45*, 553–561.
Lowenstein, T. K., Hardie, L. A., Timofeeff, M. N., & Demicco, R. V. (2003). Secular variation in seawater chemistry and the origin of calcium chloride basinal brines. *Geology*, *31*, 857–860.
Machel, H. G., & Buschkuehle, B. E. (2008). Diagenesis of the Devonian Southesk-Cairn Carbonate Complex, Alberta, Canada: Marine Cementation, Burial Dolomitization, Thermochemical Sulfate Reduction, Anhydritization, and Squeegee Fluid Flow. *Journal of Sedimentary Research*, *78*, 366–389. https://doi.org/10.2110/jsr.2008.037 Malone, M. J., Slowey, N. C., & Henderson, G. M. (2001). Early diagenesis of shallow-water periplatform carbonate sediments, leeward margin, Great Bahama Bank (Ocean Drilling Program Leg 166). *GSA Bulletin*, *113*, 881–894.
McDowell, R. R. (1995). Depositional history of a Middle Ordovician, mixed-carbonate-clasticunit- the Kanosh Formation, Eastern Great Basin, USA. Ordovician Odyssey: Short Papers for the Seventh International Symposium on the Ordovician System. 367-370.
Morse, J. W., Arvidson, R. S., & Luettge, A. (2007). Calcium carbonate formation and dissolution. *Chemical Reviews*, *107*, 342–381.
Mucci, A., & Morse, J. W. (1983). The incorporation of $Mg^{2+}$ and $Sr^{2+}$ into calcite overgrowths: Influence of growth rate and solution composition. *Geochimica et Cosmochimica Acta*, *47*, 217–223.
Nielsen, L. C., Yoreo, J. J., & DePaolo, D. J. (2013). General model for calcite growth kinetics in the presence of impurity ions. *Geochimica et Cosmochimica Acta*, *115*, 100–114.
Paul, A., & Lokier, S. W. (2017). Holocene marine hardground formation in the Arabian Gulf: Shoreline stabilisation, sea level and early diagenesis in the coastal sabkha of Abu Dhabi. *Sedimentary Geology*, *352*, 1–13.
Perry, E. A. Jr., Gieskes, J. M., & Lawrence, J. R. (1976). Mg, Ca and O18O16 exchange in the sediment-pore water system, hole 149, DSDP. *Geochimica et Cosmochimica Acta*, *40*, 413–423.
Pourmand, A., Dauphas, N., & Ireland, T. J. (2012). A novel extraction chromatography and MC-ICP-MS technique for rapid analysis of REE, Sc and Y: Revising CI-chondrite and Post-Archean Australian Shale (PAAS). *Chemical Geology*, *291*, 38–54.
Rameil, N., Immenhauser, A., Csoma, A., & Warrlich, G. (2012). Surfaces with a long history: The Aptian top Shu'aiba Formation unconformity, Sultanate of Oman. *Sedimentology*, *59*, 212–248.
Rausch, S., Böhm, F., Bach, W., Klügel, A., & Eisenhauer, A. (2013). Calcium carbonate veins in ocean crust record a threefold increase of seawater Mg/Ca in the past 30 million years. *Earth and Planetary Science Letters*, *362*, 215–224.
Rimstidt, J. D., Balog, A., & Webb, J. (1998). Distribution of trace elements between carbonate minerals and aqueous solutions. *Geochimica et Cosmochimica Acta*, *62*(11), 1851–1863.
Ryb, U., & Eiler, J. M. (2018). Oxygen isotope composition of the Phanerozoic ocean and a possible solution to the dolomite problem. *Proceedings of the National Academy of Sciences*, *115*, 6602–6607.
Schrag, D. P., Higgins, J. A., Macdonald, F. A., & Johnston, D. T. (2013). Authigenic carbonate and the history of the global carbon cycle. *Science*, *339*, 540–543.
Shinn, E. A. (1969). Submarine lithification of Holocene carbonate sediments in the Persian Gulf. *Sedimentology*, *12*, 109–144.
Sivan, O., Schrag, D. P., & Murray, R. W. (2007). Rates of methanogenesis and methanotrophy in deep-sea sediments. *Geobiology*, *5*, 141–151.
Skinner, L. C., Sadekov, A., Brandon, M., Greaves, M., Plancherel, Y., de la Fuente, M., et al. (2019). Rare earth elements in early-diagenetic foraminfer 'coatings': Pore-water controls and potential palaeoceanographic applications. *Geochimica et Cosmochimica Acta*, *245*, 118–132.

Sperling, E. A., Wolock, C. J., Morgan, A. S., Gill, B. C., Kunzmann, M., Halverson, G. P., et al. (2015). Statistical analysis of iron geochemical data suggests limited late Proterozoic oxygenation. *Nature*, *523*, 451–454.
Sun, X., Higgins, J., & Turchyn, A. V. (2016). Diffusive cation fluxes in deep-sea sediments and insight into the global geochemical cycles of calcium, magnesium, sodium and potassium. *Marine Geology*, *373*, 64–77.
Swart, P. K. (2015). The geochemistry of carbonate diagenesis: The past, present and future. *Sedimentology*, *62*, 1233–1304.
Taylor, P. D., & Wilson, M. A. (2003). Palaeoecology and evolution of marine hard substrate communities. *Earth-Science Reviews*, *62*, 1–103.
Tostevin, R., Shields, G. A., Tarbuck, G. M., He, T., Clarkson, M. O., & Wood, R. A. (2016). Effective use of cerium anomalies as a redox proxy in carbonate-dominated marine settings. *Chemical Geology*, *438*, 146–162.
Turner, J. V. (1982). Kinetic fractionation of carbon-13 during calcium carbonate precipitation. *Geochimica et Cosmochimica Acta*, *46*, 1183–1191.
Van der Ham, R. W. J. M., van Konijnenburg-van Cittert, J. H. A., & Indeheberge, L. (2007). Seagrass foliage from the Maastrichtian type area (Maastrichtian, Danian, NE Belgum, SE Netherlands). *Review of Palaeobotany and Palynology*, *144*, 301–321.
Veizer, J. (1983). Trace elements and isotopes in sedimentary carbonates. *Reviews in Mineralogy and Geochemistry*, *11*, 265–299.
Veizer, J., Ala, D., Azmy, K., Bruckschen, P., Buhl, D., Bruhn, F., et al. (1999). $^{87}Sr/^{86}Sr$, $\delta^{13}C$ and $\delta^{18}O$ evolution of Phanerozoic seawater. *Chemical Geology*, *161*, 59–88.
Veizer, J., Clayton, R. N., & Hinton, R. W. (1992). Geochemistry of Precambrian carbonates: IV. Early Paleoproterozoic (2.25 ± 0.25 Ga) seawater. *Geochimica et Cosmochimica Acta*, *56*, 875–885.
Veizer, J., & Prokoph, A. (2015). Temperatures and oxygen isotopic composition of Phanerozoic oceans. *Earth-Science Reviews*, *146*, 92–104.
Wallace, M. W., Hood, A. V. S., Shuster, A., Greig, A., Planavsky, N. J., & Reed, C. P. (2017). Oxygenation history of the Neoproterozoic to early Phanerozoic and the rise of land plants. *Earth and Planetary Science Letters*, *466*, 12–19.
Wasson, W., & Lohman, K. C. (2015). Isotopic and elemental evidence for meteoric alteration of a Pennsylvanian phylloid-algal mound, Holder Formation, New Mexico, U.S.A. *Journal of Sedimentary Research*, *85*, 6–20.
Watkins, J. M., Nielsen, L. C., Ryerson, F. J., & DePaolo, D. J. (2013). The influence of kinetics on the oxygen isotope composition of calcium carbonate. *Earth and Planetary Science Letters*, *375*, 349–360.
Westrop, S. R. (1989). Facies anatomy of an Upper Cambrian grand cycle: Bison Creek and Mistaya formations, southern Alberta. *Canadian Journal of Earth Sciences*, *26*, 2282–2304.
Wilson, M. A., & Palmer, T. J. (1992). Hardgrounds and Hardground Faunas. *University of Wales, Aberystwyth, Institute of Earth Studies Publications*, *9*, 1–131.
Zhao, M.-Y., & Zheng, Y.-F. (2017). A geochemical framework for retrieving the linked depositional and diagenetic histories of marine carbonates. *Earth and Planetary Science Letters*, *460*, 213–221.
Zhao, M.-Y., Zheng, Y.-F., & Zhao, Y.-Y. (2016). Seeking a geochemical identifier for authigenic carbonate. *Nature Communications*, *7*, 10885. https://doi.org/10.1038/ncomms10885

## Erratum

In the originally published version of this article, a contributing author was inadvertently omitted from the author list. Peter Scott contributed analyses and method development of the analytical technique to the paper. The author has now been added, and this version may be considered the authoritative version of record.